Icarus 225 (2013) 506–516

Contents lists available at SciVerse ScienceDirect

Icarus

journal homepage: www.elsevier.com/locate/icarus

The current martian cratering rate

I.J. Daubar [a,*], A.S. McEwen [a], S. Byrne [a], M.R. Kennedy [b], B. Ivanov [c]

[a] Lunar and Planetary Laboratory, University of Arizona, Tucson, AZ 85721, USA
[b] Malin Space Science Systems, P.O. Box 910148, San Diego, CA 92191, USA
[c] Institute for Dynamics of Geospheres, Russian Academy of Science, Moscow, Russia

ARTICLE INFO

Article history:
Received 28 June 2012
Revised 14 March 2013
Accepted 8 April 2013
Available online 23 April 2013

Keywords:
Cratering
Mars
Mars, Surface

ABSTRACT

The discovery of 248 dated impact sites known to have formed within the last few decades allows us to refine the current cratering rate and slope of the production function at Mars. We use a subset of 44 of these new craters that were imaged before and after impact by Mars Reconnaissance Orbiter's Context Camera – a thoroughly searched data set that minimizes biases from variable image resolutions. We find the current impact rate is 1.65×10^{-6} craters with an effective diameter $\geqslant 3.9$ m/km^2/yr, with a differential slope (power-law exponent) of -2.45 ± 0.36. This results in model ages that are factors of three to five below the Hartmann (Hartmann, W.K. [2005]. Icarus 174, 294–320) and Neukum et al. (Neukum, G., Ivanov, B.A., Hartmann, W.K. [2001]. Space Sci. Rev. 96, 55–86)/Ivanov (Ivanov, B.A. [2001]. Space Sci. Rev. 96, 87–104) model production functions where they overlap in diameter. The best-fit production function we measure has a shallower slope than model functions at these sizes, but model function slopes are within the statistical errors. More than half of the impacts in this size range form clusters, which is another reason to use caution when estimating surface ages using craters smaller than ~50 m in diameter.

1. Introduction

Nearly all planetary bodies show the scars of impact bombardment. The most visible cases are ancient, landscape-altering features, but the population of impacting material extends to the present day, and very small sizes. The relative abundances of craters have long been used to estimate crater retention ages for planetary surfaces, providing a minimum age for emplacement of major geologic units. This method assumes a spatially randomized impact flux, a calibrated size distribution of impactors, the preservation of every crater, and a temporally randomized flux over short timescales but a known (or modeled) temporal variation over long timescales. The return of dateable samples from the Moon (summary in Wilhelms et al. (1987)) led to the assignment of absolute ages to lunar crater counts (e.g. Baldwin, 1985; Neukum and Ivanov, 1994; Stöffler and Ryder, 2001). The dated samples probably correspond to the landscape's crater retention ages in the case of the lunar maria, where voluminous lava outpourings reset the crater retention age and little has happened since, except cratering. These crater age models have in turn been extended to other planetary surfaces in the inner Solar System by applying dynamical models, observations of impacting populations, differences in resulting crater sizes based on gravity and impact velocity (e.g. Ivanov, 2001), and atmospheric corrections in the case of Mars and Venus (e.g. McKinnon et al., 1997; Popova et al., 2003; Hartmann, 2005). The result is a set of cratering chronology models used widely on Mars to obtain absolute ages for landscapes (e.g. Hartmann and Neukum, 2001; Ivanov, 2001; Neukum et al., 2001; Hartmann, 2005 and previous iterations). The comparison of the modern terrestrial impact rate and young (<100 My) lunar cratering rate shows the plausibility of this approach (Ivanov, 2006). We lack dated rocks from known locations on Mars, and martian geologic history is much more complicated than that of the lunar maria. Nevertheless, dating landscapes using cratering models combined with superposition relations can provide useful constraints on interpreting the geologic history.

With the presence at Mars of higher-resolution cameras and availability of repeat imaging over time, the present-day martian bombardment rate can now be compared to these model predictions. Given the short time (geologically speaking) over which we have been observing Mars, only the smallest craters can be expected to have formed in statistically significant numbers.

Without absolute ages of rocks linked to specific locations on any Solar System bodies other than the Moon, crater counting is our only tool for measuring other surface ages. Quantifying historical bombardment can be problematic, even with dated samples (e.g. controversy over a possible ancient lunar cataclysm (e.g. Tera et al., 1974; Cohen et al., 2000; Hartmann, 1975, 2003). However,

* Corresponding author. Fax: +1 520 626 8998.
E-mail addresses: ingrid@pirl.lpl.arizona.edu (I.J. Daubar), mcewen@pirl.lpl.arizona.edu (A.S. McEwen), shane@lpl.arizona.edu (S. Byrne), mkennedy@msss.com (M.R. Kennedy), boris.ivanov@univie.ac.at (B. Ivanov).

0019-1035/$ - see front matter © 2013 Elsevier Inc. All rights reserved.
http://dx.doi.org/10.1016/j.icarus.2013.04.009

we now have definitive data on the modern impact rate at Mars, which we present here.

In addition, there has been much debate over the relative contributions of secondary versus primary craters at small crater sizes (e.g. Shoemaker, 1965; McEwen et al., 2005; McEwen and Bierhaus, 2006; Hartmann, 2007; Werner et al., 2009; Robbins and Hynek, 2011; Xiao and Strom, 2012), but we now have data on a set of craters known to represent only primary impactors.

Malin et al. (2006) reported 20 new impact sites found in a campaign of images from the Mars Orbiter Camera (MOC) on the Mars Global Surveyor. A 21,506,629 km^2 area of Mars was imaged twice with the wide-angle camera at 230 m/pixel scale, ~7 years apart. The survey was restricted to dust-mantled regions, where new impacts create dark spots ("blast zones") much larger than the crater and its ejecta. This survey found a set of 44 new dark spots; follow-up narrow-angle ~1.5 m/pixel MOC images led to the verification of 20 new impact sites that formed at various times within that period. Of those 20, the largest crater (their Site 17) was later discovered by HiRISE to contain aeolian bedforms, indicating that impact is unlikely to be as young as 7 years (Bridges et al., 2007; McEwen et al., 2007b; Golombek et al., 2010). Even excluding that site, the largest craters from that study still provided a fairly good comparison to the model isochrons of Hartmann (2005). The results indicated that the cratering rate over those 7 years roughly matched the Hartmann chronology model at ~20–30 m diameters (D) (Fig. 4). When a postulated correction to the scaled area was made to account for the statistically non-random distribution of those new impacts, the match at $D \sim 20–30$ m was even better (Kreslavsky, 2007). That non-random distribution could have been due to some areas within the dust-covered survey area being less likely to form dark spots. This analysis should be revisited with our new dataset with >10× the number of craters, as some of the former voids now contain new dark spots with craters. Note that the slope of the observed size–frequency distribution (SFD) was much "shallower" than model predictions, with fewer craters at smaller sizes, thought to be due to incomplete discoveries at small sizes (Malin et al., 2006).

In the years since, we have the added benefit of continuing repeat coverage of much of Mars, in addition to much higher-resolution imagery with which to follow up on continuing discoveries. We can now extend that test to a larger data set and smaller craters. As of February 2012, a total of 248 new impact sites have been confirmed by the High Resolution Imaging Science Experiment (HiRISE) (McEwen et al., 2007a, 2010) following their discovery by the Context Camera (CTX) (Malin et al., 2007), both on the Mars Reconnaissance Orbiter (MRO). This includes confirmation of the apparent youth of 19 of the 20 impact sites on Mars detected by Malin et al. (2006).

These impact events have occurred within the last few decades, as indicated by the absence of associated dark spots in previous images. Some of these sites have been described elsewhere (McEwen et al., 2007b, 2007c; Ivanov et al., 2008, 2009, 2010; Byrne et al., 2009; Daubar et al., 2010, 2011; Daubar and McEwen, 2009; Kennedy and Malin, 2009). This work is a summary of the new impact findings through February 2012, with a new technique to directly measure the production function (PF). As discoveries (and impacts) are ongoing, we expect this work will continue to be refined in the coming years.

2. Detection of new impacts

In our current study, possible new impact sites are initially recognized by the presence of characteristic dark spots seen in CTX images (Fig. 1). If the dark spots are not present in previous imagery of sufficient quality and resolution (drawing from various data sets spanning 30 years of martian exploration), it is considered a candidate new impact site. HiRISE then follows up on these sites to confirm a very recent impact origin, using criteria of sharp craters present with no sign of modification by aeolian or other processes, except for wind streaks, which can plausibly form in a few years since the impact event. The blast zones used for the initial detection are one to two orders of magnitude larger in diameter than the crater itself (Ivanov et al., 2010). This is fortunate since searching for new meter-size craters in HiRISE images alone would be impractical due to the limited area that could possibly be covered repeatedly at high resolution.

We interpret the dark spots as being formed by removal or redistribution of surface dust in the impact blast. Because this process is key to the initial identification of candidate new impact sites, the data set has an obvious spatial bias toward the dustiest areas of Mars (Amazonis, Tharsis and Arabia regions) (Fig. 3). This bias is accounted for by scaling the results to only those areas with repeat coverage and a minimum amount of dust cover. Only a few of the new impact sites are outside of these especially dusty regions. Conceivably, impacts onto some bright dusty areas might not actually make dark spots, so it is possible we are undercounting new impacts in these areas. It is also possible that some deep dust deposits have an albedo at depth similar to that of the surface, so an impact blast would not create a detectable dark spot. However, it is unlikely that large numbers of new impacts are not creating dark spots in these regions: some bright areas might be indurated dust, but this leads to a higher thermal inertia, whereas these regions have uniformly low thermal inertia (Christensen et al., 2001).

3. Description of impact sites

Detailed information about all 248 sites is presented in Supplemental Table 1, including the 19 sites discovered by (Malin et al., 2006) and confirmed by HiRISE. A number of unconfirmed sites were unable to be verified either as definitely new or definitely impact-related (Supplemental Table 2). Although their locations are for the most part confined to the dustiest areas of Mars (Fig. 3), diverse types of target material within those areas contribute to the wide variations in crater and ejecta morphologies and albedo patterns (Fig. 2).

Of the 248 new impact sites, 56% of them comprise clusters of individual craters. Here the impactor probably fragmented in the martian atmosphere before impacting the surface. These can be distinguished from secondary craters by their circular planforms, higher depth/diameter ratios than typical for secondaries (Daubar and McEwen, 2009), and the fact that they are not located in rays or sub-clusters radially extending from a central impact. In comparison, Malin et al. (2006) found only ~35% of their new impacts to be clusters. The discrepancy is most likely due to improved statistics and resolution. HiRISE can resolve individual craters in cases where the MOC NA only detected dark spots, for example Site 2 in Malin et al. (2006). We are able to find smaller impact sites with CTX versus MOC WA, but smaller bolides are not necessarily more likely to fragment (Popova et al., 2011). It is possible, although unlikely, that more recent impacts have differing source impactor populations with different bulk strengths or collisional histories, for example, which would affect their breakup in the atmosphere (e.g. Popova et al., 2007). Spikes in the impact flux on short timescales have been described in the lunar (Öberst and Nakamura, 1991) and terrestrial (Zappala et al., 1998) impact histories.

The smallest individual craters HiRISE can resolve are about 0.75 m (3 pixels) in diameter, but in practice, we find many craters <1 m diameter are too indistinct to reliably measure. Counts might be incomplete for craters up to several meters in diameter due to

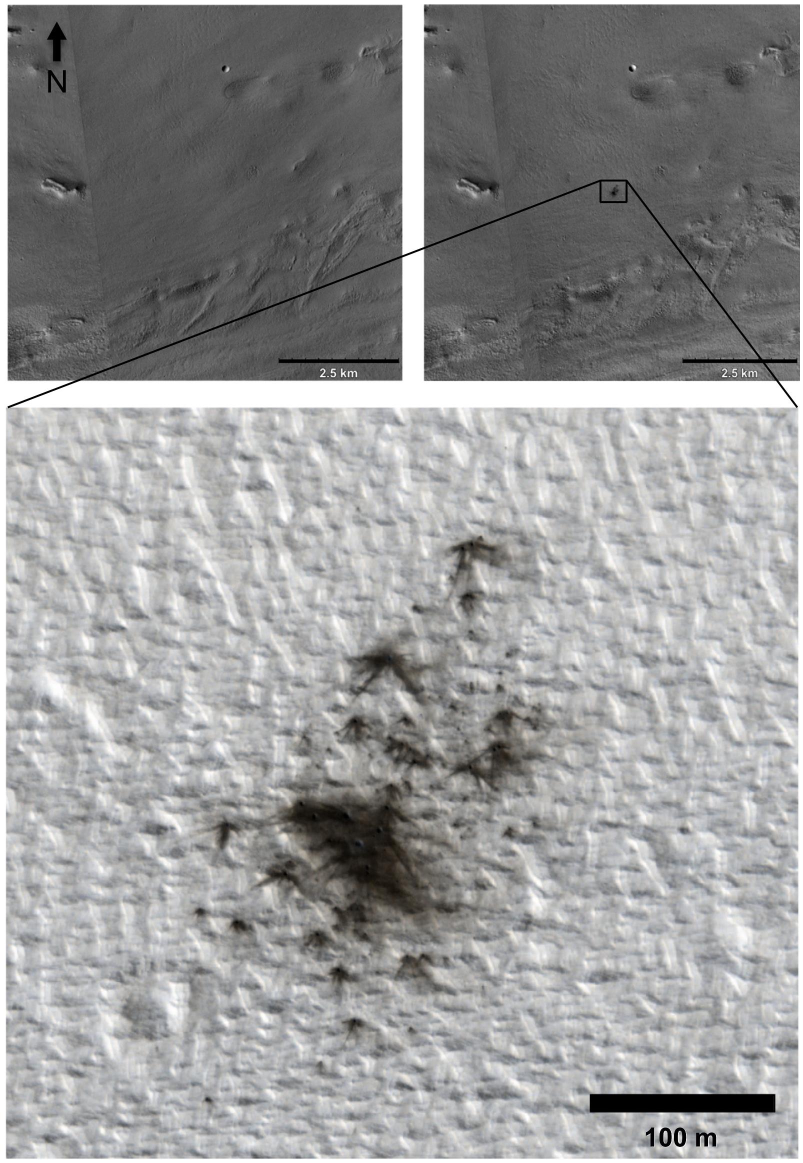

Fig. 1. One of the new impact sites located at 4.472°N, 246.893°E. CTX images G02_018995_1846_XI_04N113W (08/15/10, left) and G11_022608_1848_XI_04N113W (5/24/11, right) constrain its formation date. HiRISE enhanced color image ESP_022964_1845 (bottom) shows details of individual craters in cluster and albedo patterns surrounding the impact site. Images have been stretched for contrast. CTX image G12_022964_1845_XI_04N113W has been mosaicked with the other CTX images for regional context. HiRISE image: NASA/JPL/University of Arizona. CTX images: NASA/JPL/MSSS.

the detection technique (see Section 5.1). Golombek et al. (2008) considered HiRISE boulder counts to be complete above ~2 m diameter, so crater completeness might be similar due to image limitations (resolution, signal:noise ratio [SNR], background contrast, overlapping craters).

Several sites with newly-appearing dark spots lack visible craters in HiRISE follow-up images, although a blast zone pattern typical of other new impact sites is present (see Supplemental Table 2). We interpret these to be either aeolian redistribution and/or removal of surficial dust; or "airbursts" like the terrestrial Tunguska event (Kulik, 1927; translation Wiens and La Paz, 1935) or impact-related "radar-dark" spots on Venus (McKinnon et al., 1997), where the impactor was largely destroyed by its passage through the atmosphere, but the shock wave and small objects reached the surface and disturbed dust in a process similar to that which occurred at the sites with detected craters. There are several possible explanations for the lack of detected craters at these sites: the resulting fragments were so small that nothing large enough to form a detectable crater (>0.75 m diameter) survived to reach the surface; the individual fragments were decelerated to the point that craters did not form; or they did form, but the resulting craters are below the resolution limit of the data. There is also a possibility that these are older impact sites with unresolved craters and either "reactivated" dark spots, or with lower-quality or hazy "before" images that prevented older dark spots from being noticed. We consider it more likely that these are new airburst locations because the patterns in the dark spots are similar to our confirmed impact sites, not streaky like wind-blown patches. Regardless, we do not include these in our statistics since they have not been confirmed as impact-related in origin, and we have only an upper limit on the possible size of the craters.

In many cases, high-resolution images reveal intricate patterns in the blast zones that surround the new impact craters (Fig. 2). These patterns cannot be explained by normal ejecta dynamics, but might be described by the interaction of impact-related atmospheric shock waves (Malin et al., 2006; Ivanov et al., 2010;

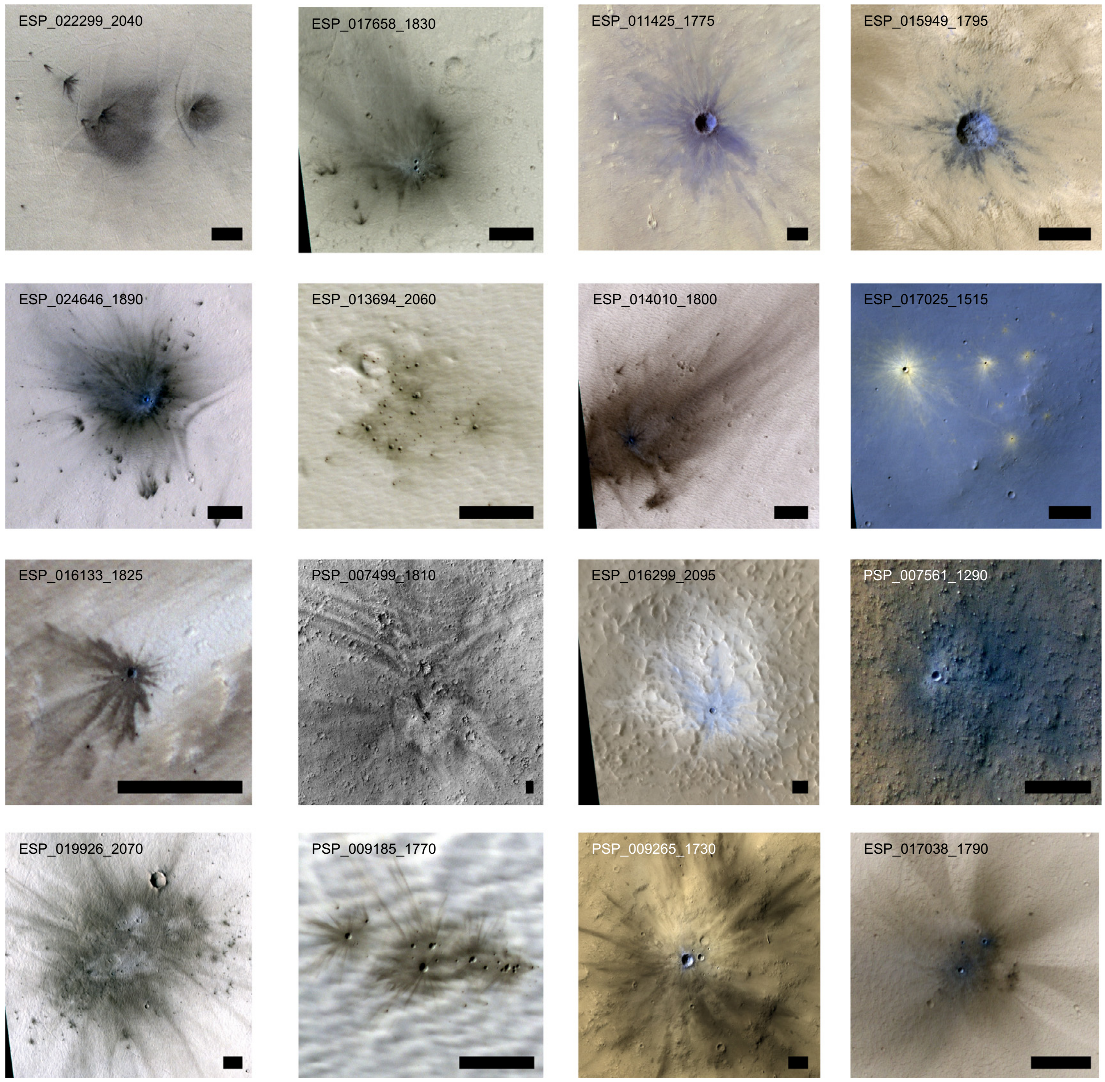

Fig. 2. Selected examples of new dated impact sites, showing a wide variety of crater and ejecta morphologies, color and albedo patterns. HiRISE observation IDs are indicated; scale bars are all 50 m. For coordinates and other details, see Supplemental information. Color images are enhanced RGB or IRB; black and white are RED filter. See McEwen et al. (2010) for more information on HiRISE data products. Images have been stretched for contrast, and north is up in all images. HiRISE images are available from the Planetary Data System or http://hirise.lpl.arizona.edu. Images: NASA/JPL/University of Arizona. (For interpretation of the references to color in this figure legend, the reader is referred to the web version of this article.)

Burleigh et al., 2012). This supports the hypothesis that the lowering of albedo forming the dark spots is due to removal or redistribution of a thin layer of bright dust (Malin et al., 2006). At some sites, meter-scale dust avalanches, presumably caused by the impact, surround the crater. These contribute to the decrease in overall albedo (Burleigh et al., 2012).

Several candidate sites, including one of the original twenty reported in Malin et al. (2006), have been found to contain aeolian bedforms or other signs of advanced age when examined at high resolution (Bridges et al., 2007; McEwen et al., 2007b). Although ripple and dune movement has been observed recently over timescales of months to years (e.g., Silvestro et al., 2010; Chojnacki et al., 2011; Bridges et al., 2012a, 2012b), the formation of new bedforms has not been observed over short timescales away from existing aeolian landforms. New ripples have been seen to form in less than 1 Mars year on fresh dune-gully aprons (Dundas et al., 2012), but they require strong winds and a large amount of unconsolidated sand-sized sediment. A new impact might produce some sand-sized material (although these new craters do not produce much ejecta in general) and act as a sink for loose material, but we have seen no evidence for this in monitoring the new impact sites over several martian years (Dubar et al., 2012). Thus craters containing well-developed bedforms are most likely older than a few decades and are not included in this study. The apparent emergence of dark spots in the few cases where aeolian bedforms are present might be due to uneven aeolian redistribution of dust in the intervening time period, they might be older dark spots that have been recently uncovered by aeolian activity, or they might have been obscured by atmospheric dust or haze in the previous image. It would take as little as 40 μm of dust re-deposition to increase the albedo to that of surrounding dust (Fischer and Pieters, 1993). A layer of dust that thin could take a short amount of time (a few martian years or decades) to deposit from airfall. Dust devil activity, the tracks of which are seen at some sites, might also contribute to changing surface albedos over short time scales. In comparison, erasure of tracks from the Mars Exploration Rovers Spirit and Opportunity has occurred over timescales of only one martian year (Geissler et al., 2010).

These new dated craters are known to be primaries and not secondaries (as Malin et al. (2006) also argued for their data set)

Table 1
Details of the 44 dated impact sites constrained before and after by CTX images. The "before" image is the latest image that clearly lacks a dark spot. The "after" image is the earliest image in which the dark spot is visible. For similar data on the complete set of new impact sites, see Supplemental information.

Site	(Effective) diameter (m)	Latitude (°N, planetocentric)	Longitude (°E)	Before image	Date of before image	After image	Date of after image	Time between before/after images (years)	HiRISE observation ID
1	4.9 ± 0.04	9.049	259.507	P09_004477_1906_X	07/11/07	P13_006178_1907_XN_10N100W	11/20/07	0.4	PSP_007246_1890
2	2.1 ± 0.1	25.604	188.579	P06_003451_2035_X	04/22/07	P13_006286_2073_XN_27N171W	11/29/07	0.6	PSP_006998_2060
3	14.7 ± 0.1	14.524	268.850	P03_002169_1937_X	01/12/07	P14_006560_1936_XN_13N091W	12/20/07	0.9	PSP_007272_1945
4	1.7 ± 0.03	−6.242	273.984	P03_002103_1721_X	01/07/07	P15_006850_1741_XN_05S086W	01/12/08	1.0	PSP_007496_1735
5	3.2 ± 0.03	−2.955	287.823	P02_001997_1744_X	12/30/06	P18_007891_1742_XN_05S071W	04/02/08	1.3	PSP_010528_1770
6	4.8 ± 0.1	15.650	266.216	P12_005558_1952_X	10/03/07	P18_007984_1959_XN_15N093W	04/09/08	0.5	PSP_010621_1960
7	6.4 ± 0.03	−1.928	233.131	P06_003344_1782_X	04/14/07	P19_008539_1776_XI_02S126W	05/22/08	1.1	PSP_010319_1780
8[b]	8.0 ± 0.4	46.351	176.891	P20_008699_2247_X	06/04/08	P22_009556_2263_XI_46N183W	08/10/08	0.2	PSP_009978_2265
9	6.6 ± 0.07	−2.021	246.574	B01_009923_1790_X	09/07/08	B01_010213_1790_XN_01S113W	09/30/08	0.1	PSP_010635_1780
10	6.0 ± 0.02	−6.019	236.034	P07_003845_1749_X	05/23/07	B05_011743_1731_XN_06S124W	01/27/09	1.7	ESP_016200_1740
11	2.5 ± 0.03	2.910	250.769	P17_007510_1851_X	03/03/08	B05_011782_1818_XI_01N109W	01/30/09	0.9	ESP_012349_1830
12	4.8 ± 0.04	11.476	255.011	P13_005954_1927_X	11/03/07	B06_012006_1912_XI_11N104W	02/17/09	1.3	ESP_013707_1915
13	11.5 ± 0.06	5.543	177.891	P02_001790_1871_X	12/13/06	B06_012022_1845_XI_04N182W	02/18/09	2.2	ESP_017969_1855
14	3.5 ± 0.04	10.599	186.484	P08_004150_1923_X	06/15/07	B07_012259_1927_XI_12N173W	03/08/09	1.7	ESP_016149_1905
15	4.6 ± 0.08	4.431	201.397	P18_008171_1829_X	04/24/08	B08_012931_1847_XN_04N158W	04/30/09	1.0	ESP_013287_1845
16	4.7 ± 0.03	−8.878	217.642	P03_002382_1705_X	01/29/07	B09_013181_1733_XN_06S142W	05/19/09	2.3	ESP_018561_1710
17[a]	33.8 ± 0.09	−0.630	248.913	P03_002394_1809_X	01/29/07	B09_013193_1810_XI_01N111W	05/20/09	2.3	ESP_015949_1795
18	6.4 ± 0.03	−6.848	259.395	P21_009250_1733_X	07/17/08	B11_013786_1729_XI_07S100W	07/05/09	1.0	ESP_016331_1730
19	6.0 ± 0.01	−4.168	246.709	P09_004438_1763_X	07/08/07	B11_014037_1761_XN_03S113W	07/25/09	2.0	ESP_016582_1760
20	8.6 ± 0.02	3.241	235.100	P13_006113_1819_X	11/15/07	B16_015989_1834_XN_03N124W	12/24/09	2.1	ESP_023426_1835
21	3.1 ± 0.09	4.865	279.362	P17_007799_1860_X	03/26/08	B17_016172_1863_XN_06N080W	01/07/10	1.8	ESP_025943_1850
22	3.6 ± 0.02	24.106	279.799	B02_010370_2044_X	10/12/08	B17_016251_2044_XN_24N080W	01/13/10	1.3	ESP_026589_2045
23	5.6 ± 0.02	−0.965	37.833	P07_003694_1797_X	05/11/07	B17_016260_1788_XN_01S322W	01/14/10	2.7	ESP_017038_1790
24	9.4 ± 0.08	30.494	178.249	P18_008119_2106_X	04/20/08	B17_016347_2105_XN_30N181W	01/21/10	1.8	ESP_017481_2110
25	4.7 ± 0.003	−2.566	183.966	B03_010901_1782_X	11/22/08	B18_016492_1798_XN_00S176W	02/01/10	1.2	ESP_018404_1775
26	6.4 ± 0.04	24.921	245.289	P20_008868_2048_X	06/17/08	B18_016516_2043_XN_24N114W	02/03/10	1.6	ESP_018784_2050
27	4.7 ± 0.02	30.791	219.235	P13_006153_2133_X	11/18/07	B18_016662_2087_XN_28N140W	02/14/10	2.2	ESP_017229_2110
28	7.1 ± 0.01	−15.346	250.627	B17_016305_1653_X	01/17/10	B18_016727_1658_XI_14S109W	02/19/10	0.1	ESP_018217_1645
29	7.6 ± 0.01	7.493	245.188	P17_007497_1865_X	03/02/08	B20_017360_1895_XI_09N115W	04/10/10	2.1	ESP_017927_1875
30	4.6 ± 0.003	12.331	271.464	P18_007997_1935_X	04/10/08	B20_017570_1913_XN_11N088W	04/26/10	2.0	ESP_018493_1925
31	3.4 ± 0.002	40.341	185.501	B17_016439_2230_X	01/28/10	B22_018140_2231_XI_43N174W	06/09/10	0.4	ESP_018707_2205
32	4.2 ± 0.04	46.611	133.706	B21_017654_2279_X	05/03/10	G01_018577_2279_XI_47N226W	07/14/10	0.2	ESP_018854_2270
33	2.7 ± 0.03	3.117	53.383			B01_009930_1835_XI_03N306W	09/08/08		
						G01_018712_1840_XI_04N306W	07/24/10	1.9	ESP_022536_1830
34	20 ± 0.05	41.017	126.301			B19_016995_2190_XN_39N233W	03/12/10		
						G02_019052_2214_XI_41N233W	08/20/10	0.4	ESP_019830_2215
35	5.4 ± 0.03	18.935	202.796	B09_013076_1989_X	05/11/09	G02_019168_1992_XN_19N157W	08/29/10	1.3	ESP_020869_1990
36	4.2 ± 0.05	32.249	112.389	B07_012288_2119_X	03/10/09	G03_019580_2127_XN_32N247W	09/30/10	1.6	ESP_020714_2125
37	3.5 ± 0.01	12.270	196.484	B19_016953_1945_X	03/09/10	G04_019788_1920_XI_12N163W	10/16/10	0.6	ESP_022056_1925
38	7.3 ± 0.02	4.472	246.893	G02_018995_1846_X	08/15/10	G11_022608_1848_XI_04N113W	05/24/11	0.8	ESP_022964_1845
39	4.2 ± 0.05	3.702	275.991	B09_012981_1844_X	05/03/09	G14_023886_1819_XN_01N083W	08/31/11	2.3	ESP_025864_1835
40	10.9 ± 0.01	24.582	291.109	P17_007693_2040_X	03/17/08	G15_024215_2048_XN_24N069W	09/26/11	3.5	ESP_028659_2050
41	11.2 ± 0.04	11.840	275.694	B17_016093_1915_X	01/01/10	G16_024482_2155_XN_35N158W	10/17/11	1.8	ESP_026009_1920
42	3.8 ± 0.07	35.318	201.373	G05_020091_2155_X	11/09/10	G16_024482_2155_XN_35N158W	10/17/11	0.9	ESP_026038_2155
43	9.0 ± 0.07	3.290	246.827	B02_010424_1849_X	10/16/08	G17_024942_1813_XI_01N112W	11/22/11	3.1	ESP_027975_1835
44	11.8 ± 0.09	2.579	248.522	B09_013193_1810_X	05/20/09	G18_025087_1836_XI_03N111W	12/03/11	2.5	ESP_026221_1825

[a] This impact site is even more strictly date-constrained by MARCI images P16_007220_0298_MA_00N109W and P16_007365_0349_MA_00N109W, but is included in the statistics since it would have been detected in these CTX images with or without the existence of the MARCI data.

[b] Reported in Byrne et al. (2009).

because they formed at different times, in widespread locations across the planet. No new large craters have been found that could be the potential primary or primaries if these were secondaries; such a new crater would almost certainly have been detected by at least one of the eight cameras orbiting Mars on four spacecraft over the past decade. In addition, the statistical probability of enough new large impact events occurring within the last decade to explain these as secondaries is extremely low.

4. Methods

4.1. Constraining formation dates

The formation date of each confirmed impact site is constrained using previously-acquired images of Mars. The formation date is bracketed by the dates of the latest image of sufficient resolution that lacks a dark spot (the "before" image) and the earliest image in which the spot is visible (the "after" image). The after image is not necessarily the discovery image, since after finding a dark spot, previous data are searched for the possibility of tighter time constraints. See Table 1 for constraining images and dates for the 44 impacts with CTX before- and after-images we use to measure the production function, and Supplemental information for data on the remaining new impacts.

4.2. Diameter measurements

Crater diameters were measured from rim to rim in the image processing software package ENvironment for Visualizing Images (ENVI, 1998). Airbursts and unresolved craters (<3 HiRISE pixels) were not included. Diameters were measured three times and the results averaged to estimate measurement errors, which were less than a pixel (0.25 m). Craters in clusters were measured individually, down to the limit of the image's resolution. To approximate the diameter of the crater that would have formed had the impactors not broken up in the atmosphere, effective diameters were calculated for clusters using (Malin et al., 2006; Ivanov et al., 2009):

$$D_{\text{eff}} = \left(\sum_i D_i^3\right)^{1/3}$$

This assumes pure "strength" scaling of the individual impacts. Fragmentation modeling indicates that this is a good approximation for $D_{\text{eff}} \sim 10$ m and larger, while for smaller impactors ~1 m, D_{eff} is underestimated by ~15% (Williams et al., 2012).

4.3. Calculating the area–time factor

In order to find the most robust estimate of the current impact rate, we limited the data set to those 44 craters whose formations are constrained by CTX data for both before and after images. This ensures consistent data quality: results are not biased by lower detection limits of other data sets. It also provides some guarantee of completeness, since every CTX image in dusty regions has been examined for new dark spot features.

To understand the current rate of impacts in terms of a production function, an area to which to scale the size–frequency distribution of craters is required. Typically in crater counting, this would be the area over which all craters were counted. However, the CTX–CTX image overlaps vary in time as well as area, so a new approach is needed. Thus, we scale the number of craters in a given diameter size bin by a composite area–time factor (ATF):

$$\text{ATF} = \sum_i a_i \Delta t_i$$

The ATF was calculated by dividing the planet into small geographic elements. CTX coverage of each element was queried and the element area (a) was multiplied by the time elapsed between the earliest and most recent images (Δt) at that location. This method ensures that areas covered by more than two images are not double-counted. The sum of all of these area–time products is the ATF, a factor that represents the total area × time in which it was possible to have found any new craters. To account for the lack of detections over non-dusty areas, we only included locations with a dust cover index (DCI) (Ruff and Christensen, 2002) value $\leqslant 0.96$ (Fig. 3). The DCI is the average Thermal Emission Spectrometer (TES) emissivity from 1350 to 1400 cm^{-1}, a measure of the depth of the spectral feature that is most sensitive to particle size. Areas with DCI > 0.96 have relatively little dust cover, so impacts there might not form a detectable dark spot.

Only CTX images between 60°S and 60°N degrees latitude were included, since new craters are difficult to find at high latitudes where seasonal "repainting" of albedo patterns complicates their detection. Images taken at incidence angles of greater than 80°, pixel scales greater than 15 m/pixel, and calibration images were also excluded, since they would not be consistently useful for finding new dark spots. There is no automated way to identify all low-quality CTX images, for example those with atmospheric obscuration of the surface. To be conservative, we therefore excluded all images from MRO orbits 4346–4741, which spanned the 2007 global dust event. For comparison, outside of this dust storm period, we have found only 2.8% of HiRISE images to be affected even a small amount by atmospheric haze, let alone surfaces significantly obscured by the atmosphere. Although CTX images typically have a lower SNR than HiRISE images, we estimate that only 1–5% of CTX images are too hazy to see new dark spots on the surface: ~5% of all CTX images, but only ~1% of those over the dusty areas where we see dark spots. Therefore, the resulting set of CTX images we use to calculate the ATF should represent, to within a few percent, all of the images in which it has been possible to detect a new dark spot. In other words, only a few percent of new impacts might have been missed within this set of images. The value we calculated for the ATF is 19,718,204 km^2 yr.

The result of dividing the number of new craters by the ATF is the number of new craters per area, per year, which is equivalent to the 1 year production function (PF). Since this is an unusual approach, it is helpful to consider the limiting case: one pair of images, exactly overlapping, with one new crater detected in the later of the two images. It can be seen in that case that the number of new craters produced per year per area is one divided by the area of the images, divided by the number of years elapsed between them, or 1/ATF.

To compare previous results, the Malin et al. (2006) survey was treated similarly. In this simpler case, two before- and after-surveys of 21,506,629 km^2 were conducted ~6.7 years apart. The ATF in that case is simply the survey area multiplied by the mean time between surveys, 143,499,219 km^2 yr. The PF from this method can then be directly compared to ours (Fig. 4).

5. Results and discussion

5.1. Measured current production function and comparison to models

Previously estimated rates of the number of impacts/km^2/yr (Kennedy and Malin, 2009; Daubar et al., 2010, 2011) made several simplifying assumptions – most importantly that they were detecting every new impact (larger than some detection limit) that occurred over broadly defined dusty regions of Mars, which is certainly not the case. Our area–time scaling factor takes into account the actual area and time period over which detections were possible, yielding an accurate cratering rate. To compare the detailed size–frequency relationship with established production function models, the diameters (or effective diameters for clusters) of 44 new craters with CTX before- and after-images were binned in standard $\sqrt{2}$ diameter bins and scaled to the area–time factor discussed above. Comparison with 1-year isochrons from model production functions (Hartmann, 2005; Neukum et al., 2001; Ivanov, 2001) is shown in Fig. 4. The measured production function has 1.65×10^{-6} cumulative craters with $D \geqslant 3.9$ m forming per km^2/yr. The measured PF is steeper than that of the full dataset of 248 dated sites, indicating we have reduced size biases that would be introduced if we had used all date-constraining data sets.

Our measured cratering rate falls below both of the model production functions except at the largest size bin. (It should be noted the two largest size bins contain only one impact site each.) The least squares fit slope of our new impact differential PF for $D \geqslant 3.9$ m is -2.45 ± 0.36. This is shallower than the best fit slope of either model (the Hartmann (2005) model has a differential slope of -3.2 for $3.9\text{ m} \leqslant D \leqslant 31$ m; the Neukum et al. (2001) model has a differential slope of -4.2 for $16\text{ m} \leqslant D \leqslant 31$ m). This preliminary result supports the hypothesis that the primary production function for small craters is significantly less "steep" (smaller negative power-law exponent) than that of secondary craters in this size range (e.g., Wilhelms et al., 1987; Xiao and Strom, 2012). However, the statistical error bars are large and we cannot reject the hypothesis that either of the model production functions match the slope in this size range, although it is unlikely.

The effective diameter calculation underestimates the diameter slightly for the smallest craters (~15% at 1 m) (Williams et al., 2012). Correcting for this would yield a slightly steeper SFD for $D < 10$ m. For strength-dominated craters like these, target

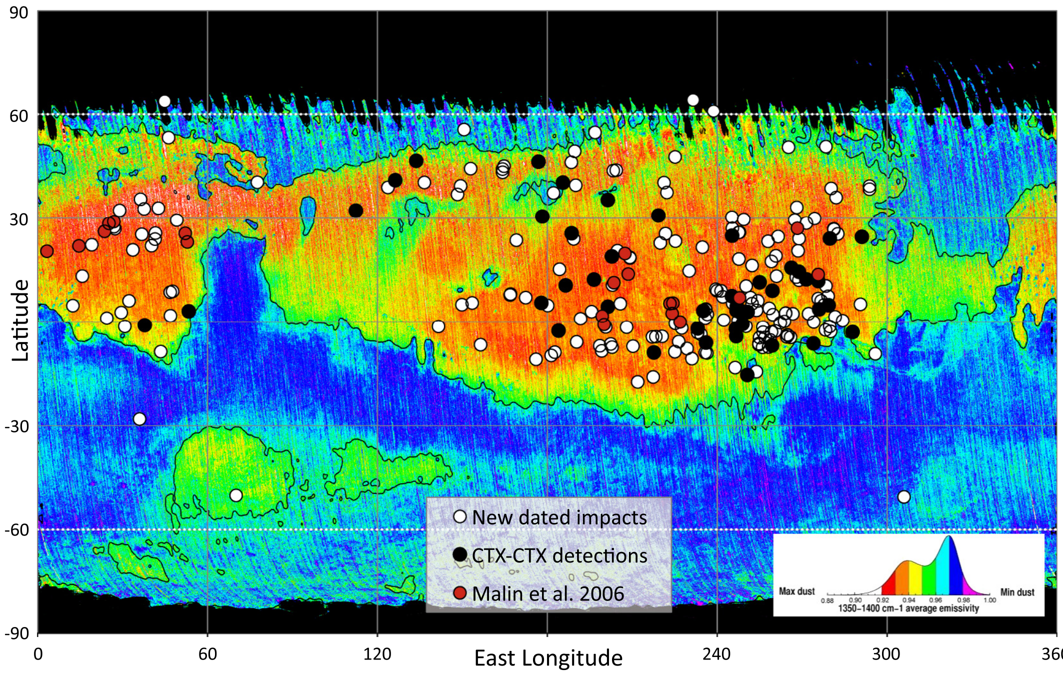

Fig. 3. Locations of 248 new dated impact sites on Mars, shown on a map of the Thermal Emission Spectrometer dust cover index (Ruff and Christensen, 2002). The 19 sites previously reported in Malin et al. (2006) that have been confirmed are shown, as are the subset of 44 sites constrained by CTX before- and after-imaging. Areas considered in our study are outlined by a contour at a dust cover index of 0.96 and latitude limits of 60°N–60°S (dotted white lines).

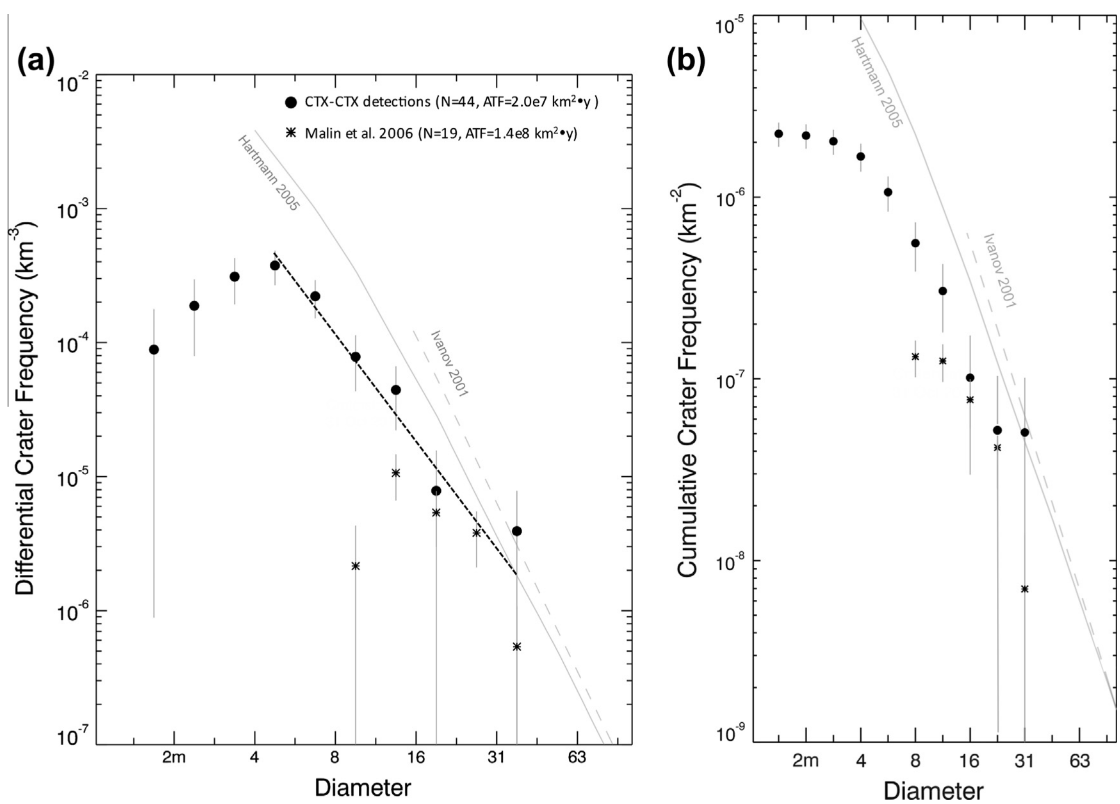

Fig. 4. Current martian production function (PF): (a) differential and (b) cumulative size–frequency diagrams of 44 new dated impact sites constrained by CTX images, scaled to the area–time function (ATF) discussed in the text (circles). Models of the 1-year PF from Hartmann (2005) using the chronology function (CF) from Hartmann (2005) as derived by Werner and Tanaka (2011) (solid gray line) and the 1-year PF from Neukum et al. (2001) using the conversion to Mars and CF from Ivanov (2001) (dashed gray line) are shown for comparison. The Malin et al. (2006) sites are also shown (stars), with crater diameters remeasured using HiRISE images, and excluding their Site 17, which is most likely not new. Also shown is the least-squares power law fit for the new impacts for $D > 3.9$ m, which has a slope of -2.45 ± 0.36. For all SFDs presented: Effective diameters were calculated for clusters as discussed in the text, and craters are in $\sqrt{2}$ diameter bins. All plots were created with the Craterstats2 program (Michael and Neukum, 2010; http://hrscview.fu-berlin.de/craterstats.html).

material properties also become important. All of these craters formed in dusty areas, but in some areas the dust is only present as a thin surface layer, while at other sites there might be a significant mantling layer of lower porosity that could be up to meters thick, for example, indurated dust or brecciated bedrock. An impact of a given energy into weaker material produces larger craters (Chapman et al., 1970), an effect that becomes more important for smaller craters (e.g., Dundas et al., 2010). However, target material with high porosity produces smaller craters (Housen and Holsapple, 2003). The potential variation in crater diameter from these uncertainties is ~20%.

Applying the Hartmann (2005) model to craters with $D > 3.9$ m yields a model age of 0.21 ± 0.06 years (the error bars we cite are the standard errors; the actual uncertainties in model ages are much larger, as we hope to demonstrate). In other words, our measured production function differs from the Hartmann model by a factor of 0.21. We use the chronology function from Hartmann (2005) as derived in Werner and Tanaka (2011): $N(D \geqslant 1\ \text{km}) = 4.4246 \times 10^{-14}(e^{6.93T} - 1) + 6.8158 \times 10^{-4}T$ (where T is in Gy). The Neukum/Ivanov model (Neukum's lunar PF as scaled to Mars by Ivanov (2001)) yields 0.29 ± 0.29 years for this data set, using only the three bins $D \geqslant 15.6$ m where the model and our data overlap. This uses the Ivanov (2001) chronology function: $N(D \geqslant 1\ \text{km}) = 2.68 \times 10^{-14}(e^{6.93T} - 1) + 4.13 \times 10^{-4}T$. Note that comparing even smaller diameters to an extrapolated Neukum/Ivanov model results in an even larger discrepancy. Unlike the Hartmann (2005) iteration, the Neukum PF was constructed for craters large enough not to be affected by the atmospheric passage of the projectile, so it does not include the "Popova correction" (Popova et al., 2003) that Hartmann made in 2005 for ablation during the projectile's passage through the atmosphere. The Neukum/Ivanov PF thus presents a reasonable upper limit of lunar-derived production flux for a conditional atmosphere-less Mars, so it is unsurprising that it falls above the Hartmann PF at these sizes. Projectiles of the size we are discussing are likely to be affected by atmospheric loss, so the Neukum PF is less appropriate, although we include both for comparison.

5.2. Discussion

Considering the many assumptions needed to produce the model PFs, the agreement between these new impact data and previous model predictions is quite good. This has also been noted about the Malin et al. (2006) results by previous workers (Ivanov and Hartmann, 2007; Hartmann, 2007; Neukum et al., 2010), although our improved statistics and extended range of diameters reveal a divergence between the models and the current measured impact rate that increases at smaller diameter. From our results, one might conclude that model ages based on craters in the ~10–50 m size range should be increased by a factor of ~three (Ivanov/Neukum model) to ~five (Hartmann model), and even larger factors at smaller diameters. However, the situation is probably not that simple. The difference could be due to several factors in addition to imperfect models:

(1) For small craters in the strength regime, the uncertainties in crater scaling due to variations in target strength translate into surprisingly large differences in model crater retention ages (Dundas et al., 2010).

(2) It is possible that we could be missing new impacts that do not form detectable dark spots, even in dusty areas. We are near the resolution limits for these sizes, especially below ~4 m where the SFD turns over. The relevant limiting detection capability is not HiRISE's, which would have no problem resolving a 4-m feature, but rather that of the lower-resolution and lower-signal-to-noise data used in the initial discoveries of the sites. In this subset of the new craters, the relevant dataset is that of CTX (6 m/pixel) with a typical SNR ~ 100:1 over bright regions (Malin et al., 2007), but the SNR for surface features can be much lower when the atmospheric opacity is high. Identification is of the dark spot, however, not the crater itself, so a given resolution limit leads to a rollover at a much smaller crater diameter. The 4-m crater diameter rollover corresponds to ~40–400 m dark spots (Ivanov et al., 2010), which would be ~7–70 CTX pixels. Dark spots smaller than 7 pixels might be difficult to recognize in CTX images when the air is dusty or hazy. Also, it's uncertain how long the dark spots persist, although the majority of non-polar impact sites show few changes when imaged repeatedly over several Mars years.

(3) Another factor in the rollover might be atmospheric ablation and deceleration at small sizes. The rollover is close to that predicted by Popova et al. (2003), who calculated atmospheric effects would lead to a depletion of craters <0.3–5 m in diameter. Although the Hartmann, 2005 PF includes a correction for this, it might not be an adequate adjustment, especially for clusters of impacts, which are not considered in Popova et al. (2003). Chappelow and Sharpton (2005) found that even larger diameters are affected by the current martian atmosphere. Their model predicts a reduction in the SFD (mostly due to diameter "bin-hopping" as impactors are reduced in size) by an order of magnitude at $D \sim 3$ m. Atmospheric effects are less significant with increasing crater diameter, becoming negligible for $D > 100$ m. This is roughly the type of discrepancy we see between our observed PF and the Neukum/Ivanov model (Fig. 4), which is based on an airless lunar cratering record. However, Chappelow and Sharpton (2005) also predicted very little fragmentation in the current atmosphere, which is very different from the 56% fragmentation that we observe, so that model might not be describing all of the relevant processes. Ablation should affect clusters more strongly: all other things being equal, individual fragments would be expected to experience more relative ablation per unit volume than an unbroken impactor, since mass loss due to ablation is proportional to cross-sectional area (e.g. Allen and James, 1964). Small bodies would also be decelerated more since they have larger surface area to mass ratios. In addition, the vertical impact velocity is reduced by atmospheric breakup, due to the addition of some amount of transverse velocity (Artemieva and Shuvalov, 2001), although this is probably a very small effect. Lastly, if fragment sizes or velocities result in crater sizes below HiRISE resolution, we would expect to see reduced effective diameters due to the omission of the smallest craters. This is, however, a small effect due to the cubed contribution of individual diameters in a cluster, so there would need to be a very large number of unresolved craters to have a significant impact on the summed effective diameter. The SFD of individual craters within clusters varies significantly from cluster to cluster, but the overall differential slope of individual craters at all of the CTX–CTX sites is −3.07 (Fig. 6). If that slope extends to smaller sizes, unresolved craters might make a significant contribution to the effective diameter. If any of these three effects were significant, the effect would be seen at the smallest-diameter end of the SFD, which would be deficient for clusters relative to single-crater sites. There is some indication of this at diameters less than 4 m (Fig. 5), but the statistics are not very robust. The SFDs for clusters' effective crater diameters and single-crater site diameters are within the error bars of each other, indicating that there is not a strong reduction of effective diameters for clusters due to atmospheric or other

effects. Differences between the two data sets are probably due to insufficient sampling. If the slightly lower number of cluster sites at the smallest diameters is real, however, it could be due to atmospheric or resolution effects affecting fragments more strongly than unbroken impactors.

(4) The discrepancy between measured and model production functions might also be due to the contribution of secondaries to models based on older surfaces. The Hartmann model explicitly includes "spatially random" secondaries, whereas the Neukum model excludes "obvious" secondaries (hence, probably also includes spatially random secondaries). Our measured PF is based on a population of known primaries, so any secondary contamination is excluded. Distant secondaries are more spatially random and are difficult to identify as secondaries; we know that distant secondaries are abundant on the Moon, Mars (e.g. McEwen and Bierhaus, 2006), and Mercury (Strom et al., 2011). A close match to the model might suggest that the model isochrones do not in fact have significant unaccounted-for secondary contamination at these sizes, if the present cratering rate matches that over the past ~3 Gy. Thus the amount by which our measurements are below the model PFs could represent the contribution from distant secondaries.

Our best-fit SFD slope supports the hypothesis that small primary craters have a "flatter" (smaller negative power-law exponent) SFD than that of unrecognized secondaries and primaries combined. This idea was first presented (and rejected) by Shoemaker (1965), but has been championed by subsequent workers (e.g., Wilhelms et al., 1987; Xiao and Strom, 2012). Our primary SFD for Mars can also be compared to those on small bodies unlikely to be contaminated by secondaries due to their low escape velocities. The martian satellites both have slightly steeper differential slopes of ~−2.9 for craters 44 m to 10 km (Phobos) and 31 m to 1.8 km (Deimos) (Thomas and Veverka, 1980). The main-belt asteroid Gaspra exhibits an even steeper fresh-crater SFD, with a differential slope of −4.3 for 0.2–0.6 km diameter craters (Chapman et al., 1996). These differences could represent differing impact populations within the main belt, a greater level of atmospheric filtering on Mars than previously modeled, or just a difference in slope at the diameters we are studying, since no previous studies have included craters this small.

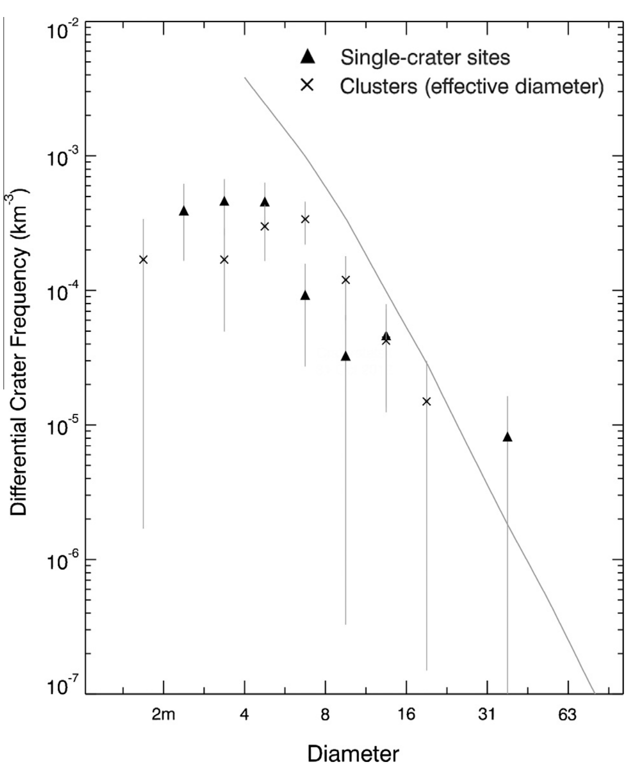

Fig. 5. Size–frequency diagram of clustered impact sites (effective diameters) (×) compared to single-crater sites (triangles). SFDs are scaled by a fraction of the ATF proportional to the amount of each type of site. The 1-year production function of Hartmann (2005) is shown for comparison, as in Fig. 4.

(5) Another possible explanation for misfit of models to the data is variation over relatively short timescales of the SFD of the primary population, which could vary as a function of asteroidal impacts, breakup, and subsequent orbital evolution including the Yarkovsky effect.

(6) Lastly, in our study, clusters of craters representing a single impact event are easily identifiable, whereas an examination of the same scene without the unifying dark spot surrounding the cluster might result in craters within a cluster being mistaken for individual primaries. This would steepen the slope of the SFD and mistakenly increase the resulting model age. Fig. 6 demonstrates the resulting SFD one might measure if the shared impact origins of clusters were unknown, for example if before/after images were not available, or if the dark spot surrounding the cluster had faded. The slope of the differential SFD is steepened from −2.45 to −3.07 ± 0.14 (including smaller diameters, 1.9 m ⩽ D ⩽ 12 m), and the resulting model age is increased by more than a factor of two, from to 0.21 to 0.48 ± 0.07 years (Hartmann, 2005, same model as discussed in Section 4.1). The rollover also occurs at smaller sizes, since the limiting resolution in that case is HiRISE's 0.25-cm pixel scale rather than that of lower-resolution imaging used to initially identify new dark spots. This implies that craters of the size we are considering – smaller than ~30 m diameter – cannot be used for dating unless the error bars are adjusted accordingly.

In summary, our results do not disprove the model PFs of Neukum et al. (2001) and Hartmann (2005), but they do show that order-of-magnitude uncertainties persist, especially at small diameters.

5.3. Is the current cratering rate representative of geologic time?

If the best-fit SFD slope we observe, which is shallower than model PFs, is extrapolated to larger craters, the conclusion would be that the current cratering rate is higher than model predictions for craters larger than D ~ 25 m – models which are based on long-term trends over geologic time. Whether or not the current rate is close to the long-term average is unknown. It could be, if the present-day PF (including secondaries) is actually as steep as the models from ~10 m to 1 km sizes, but we have no new kilometer–diameter craters with which to test that. If today's production function is in fact shallower, then we must be in the midst of a higher-than-average cratering rate, perhaps a short-term spike related to recent asteroidal collisions. Improved statistics, expected over the next few years of continued observations by MRO, are needed to verify the present-day SFD slope.

Another problem with comparing the current impact rate with the historical one is the periodic cycling of Mars's orbital eccentricity (Ivanov, 2001). This could affect the impact rate over time, as the amount of time the planet spends in proximity to the main asteroid belt changes. The current eccentricity of the martian orbit (e ~ 0.09) is large in comparison with the long-term (> a few My) average value of e ~ 0.05 (e.g. Armstrong et al., 2004; Laskar et al., 2004) (known because of the chaotic nature of the variation).

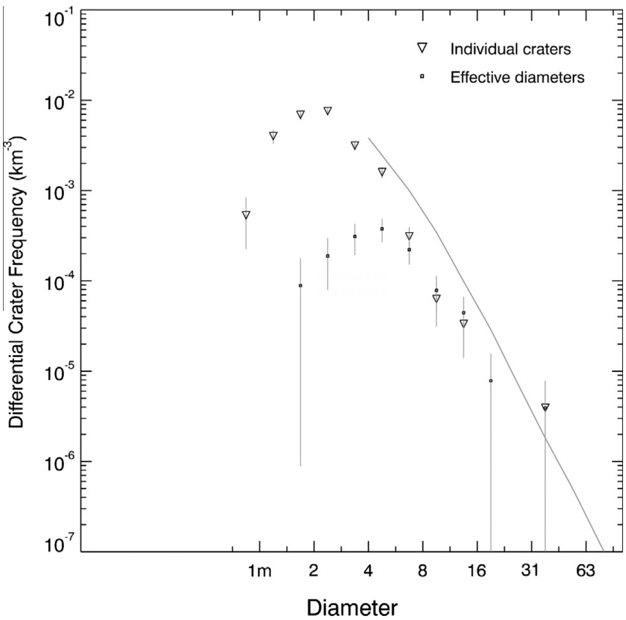

Fig. 6. Size–frequency diagram for comparison with PF presented in Fig. 4 (dots), but treating individual craters in a cluster as separate impacts (triangles). The 1-year production function of Hartmann (2005) is shown for comparison, as in Fig. 4.

If one assumes the stable Mars-crossers' orbital configurations, it means that the long-term averaged impact rate is a factor of about two less than the modern impact rate we measure (Ivanov, 2001; Ivanov and Hartmann, 2007). If this is the case, the discrepancy between ages derived from the present-day impact rate and model PFs increases by another factor of two, to about an order of magnitude for 4–50 m craters.

6. Conclusions

New meter- to decameter-sized craters on Mars are currently forming at a measurable rate: 1.65×10^{-6} craters with effective $D \geqslant 3.9$ m/km^2/yr. The modern production function is lower than model production functions commonly used to estimate crater retention ages on Mars. The current PF results in model ages that are lower by a factor of ~three than the Neukum et al. (2001) model, and a factor of ~five lower than the Hartmann (2005) model. This is within the proposed error bars of a factor of 10 that Hartmann puts on model age estimates using craters smaller than ~100 m in diameter (Hartmann, 2005). When long-term variation in orbital eccentricity is taken into account, we estimate the discrepancy is an order of magnitude. It is surprising that we find even this close of a match, however, given the origins of the models – they have been extrapolated from the lunar cratering record for larger craters (much larger in the case of Hartmann) and extended to a different planet! The near-agreement might yet be an accident if the current impact rate is not close to typical of geologic time, i.e. we cannot rule out short-term fluctuations smaller than an order of magnitude. It is too early to say whether our new observations can be reliably compared with small crater populations on older surfaces. Future multi-decade observations of larger crater formation will improve our knowledge of the primary cratering SFD on Mars. Until then, the published martian isochrons should be used with great caution for small craters. Our current impact rate statistics provide the best empirical isochrons, but they still include uncertainties of at least an order of magnitude.

Acknowledgments

This study could not have been done without the help of the HiRISE and CTX operations teams who meticulously searched images for dark spots and carefully planned coordinated follow-up observations. We are grateful to Colin Dundas for helpful comments. Stephanie Werner and an anonymous reviewer provided constructive reviews. Many thanks to Greg Michael for answering numerous questions about the workings of the Craterstats program. This work was funded by the NASA Mars Reconnaissance Orbiter project.

Appendix A. Supplementary material

Supplementary data associated with this article can be found, in the online version, at http://dx.doi.org/10.1016/j.icarus.2013.04.009.

References

Allen, H.J., James, N.A., 1964. Prospects for Obtaining Aerodynamic Heating Results from Analysis of Meteor Flight Data. NASA Technical Note D-2069.
Armstrong, J.C., Leovy, C.B., Quinn, T., 2004. A 1 Gyr climate model for Mars: New orbital statistics and the importance of seasonally resolved polar processes. Icarus 171, 255–271. http://dx.doi.org/10.1016/j.icarus.2004.05.007.
Artemieva, N.A., Shuvalov, V.V., 2001. Motion of a fragmented meteoroid through the planetary atmosphere. J. Geophys. Res. 106, 3297–3310. http://dx.doi.org/10.1029/2000JE001264.
Baldwin, R.B., 1985. Relative and absolute ages of individual craters and the rate of infalls on the Moon in the post-Imbrium period. Icarus 61, 63–91.
Bridges, N.T. et al., 2007. Windy Mars: A dynamic planet as seen by the HiRISE camera. Geophys. Res. Lett. 34, 23205. http://dx.doi.org/10.1029/2007GL031445.
Bridges, N.T., Ayoub, F., Avouac, J.-P., Leprince, S., Lucas, A., Mattson, S., 2012a. Earth-like sand fluxes on Mars. Nature 485, 339–342. http://dx.doi.org/10.1038/nature11022.
Bridges, N.T. et al., 2012b. Planet-wide sand motion on Mars. Geology 40, 31–34. http://dx.doi.org/10.1130/G32373.1.
Burleigh, K.J., Melosh, H.J., Tornabene, L.L., Ivanov, B., McEwen, A.S., Daubar, I.J., 2012. Impact airblast triggers dust avalanches on Mars. Icarus 217, 194–201. http://dx.doi.org/10.1016/j.icarus.2011.10.026.
Byrne, S. et al., 2009. Distribution of mid-latitude ground ice on Mars from new impact craters. Science 325, 1674. http://dx.doi.org/10.1126/science.117530.
Chapman, C.R., Mosher, J.A., Simmons, G., 1970. Lunar cratering and erosion from Orbiter 5 photographs. J. Geophys. Res. 75, 1445–1466. http://dx.doi.org/10.1029/JB075i008p01445.
Chapman, C.R., Veverka, J., Belton, M.J.S., Neukum, G., Morrison, D., 1996. Cratering on Gaspra. Icarus 120, 231–245.
Chappelow, J.E., Sharpton, V.L., 2005. Influences of atmospheric variations on Mars's record of small craters. Icarus 178, 40–55. http://dx.doi.org/10.1016/j.icarus.2005.03.010.
Chojnacki, M., Burr, D.M., Moersch, J.E., Michaels, T.I., 2011. Orbital observations of contemporary dune activity in Endeavor crater, Meridiani Planum, Mars. J. Geophys. Res. 116, E00F19. http://dx.doi.org/10.1029/2010JE003675.
Christensen, P.R. et al., 2001. Mars Global Surveyor Thermal Emission Spectrometer experiment: Investigation description and surface science results. J. Geophys. Res. 106, 23823–23872. http://dx.doi.org/10.1029/2000JE001370.
Cohen, B.A., Swindle, T.D., Kring, D.A., 2000. Support for the lunar cataclysm hypothesis from lunar meteorite impact melt ages. Science 290, 1754–1756.
Daubar, I.J., McEwen, A.S., 2009. Depth to diameter ratios of recent primary impact craters on Mars. Lunar Planet. Sci. 40. Abstract 2419.
Daubar, I.J., McEwen, A.S., Byrne, S., Dundas, C.M., Kennedy, M., Ivanov, B.A., 2010. The current martian cratering rate. Lunar Planet. Sci. 41. Abstract 1978.
Daubar, I.J. et al., 2011. New craters on Mars and the Moon. Lunar Planet. Sci. 42. Abstract 2232.
Daubar, I.J., Geissler, P.E., McEwen, A.S., Dundas, C.M., Byrne, S., 2012. Repeat observations of new impact sites on Mars: Changes in blast zones. AGU Fall Meeting (abstract).
Dundas, C.M., Keszthelyi, L.P., Bray, V.J., McEwen, A.S., 2010. Role of material properties in the cratering record of young platy-ridged lava on Mars. Geophys. Res. Lett. 37, 12203. http://dx.doi.org/10.1029/2010GL042869.
Dundas, C.M., Diniega, S., Hansen, C.J., Byrne, S., McEwen, A.S., 2012. Seasonal activity and morphological changes in martian gullies. Icarus 220, 124–143. http://dx.doi.org/10.1016/j.icarus.2012.04.005.
ENVI, 1998. ENVI Programmer's Guide. Research System, Inc. 930pp.
Fischer, E.M., Pieters, C.M., 1993. The continuum slope of Mars – Bidirectional reflectance investigations and applications to Olympus Mons. Icarus 102, 185–202. http://dx.doi.org/10.1006/icar.1993.1043.
Geissler, P.E. et al., 2010. Gone with the wind: Eolian erasure of the Mars rover tracks. J. Geophys. Res. 115, E00F11. http://dx.doi.org/10.1029/2010JE003674.

Golombek, M.P. et al., 2008. Size–frequency distributions of rocks on the northern plains of Mars with special reference to Phoenix landing surfaces. J. Geophys. Res. 113, E00A09. http://dx.doi.org/10.1029/2007JE003065.
Golombek, M. et al., 2010. Constraints on ripple migration at Meridiani Planum from Opportunity and HiRISE observations of fresh craters. J. Geophys. Res. 115, E00F08. http://dx.doi.org/10.1029/2010JE003628.
Hartmann, W.K., 1975. Lunar 'cataclysm' – A misconception. Icarus 24, 181–187.
Hartmann, W.K., 2003. Megaregolith evolution and cratering cataclysm models – Lunar cataclysm as a misconception, 28 years later. Meteorit. Planet. Sci. 38, 579–593.
Hartmann, W.K., 2005. Martian cratering 8: Isochron refinement and the chronology of Mars. Icarus 174, 294–320.
Hartmann, W.K., 2007. Martian cratering 9: Toward resolution of the controversy about small craters. Icarus 189, 274–278.
Hartmann, W.K., Neukum, G., 2001. Cratering chronology and the evolution of Mars. Space Sci. Rev. 96, 165–194.
Housen, K.R., Holsapple, K.A., 2003. Impact cratering on porous asteroids. Icarus 163, 102–119. http://dx.doi.org/10.1016/S0019-1035(03)00024-1.
Ivanov, B.A., 2001. Mars/Moon cratering rate ratio estimates. Space Sci. Rev. 96, 87–104.
Ivanov, B.A., 2006. Earth/Moon impact rate comparison: Searching constraints for lunar secondary/primary cratering proportion. Icarus 183, 504–507. http://dx.doi.org/10.1016/j.icarus.2006.04.004.
Ivanov, B.A., Hartmann, W.K., 2007. Exogenic dynamics, cratering and surface ages. In: Schubert, G. (Ed.), Treatise on Geophysics, vol. 10. Elsevier, Amsterdam, pp. 207–242.
Ivanov, B.A., Melosh, H.J., McEwen, A.S., HiRISE Team, 2008. Small impact crater clusters in high resolution HiRISE images. Lunar Planet. Sci. 39. Abstract 1221.
Ivanov, B.A., Melosh, H.J., McEwen, A.S., HiRISE Team, 2009. Small impact crater clusters in high resolution HiRISE images – II. Lunar Planet. Sci. 40. Abstract 1410.
Ivanov, B.A., Melosh, H.J., McEwen, A.S., HiRISE Team, 2010. New small impact craters in high resolution HiRISE images – III. Lunar Planet. Sci. 41. Abstract 2020.
Kennedy, M.R., Malin, M.C., 2009. 100 New impact crater sites found on Mars. AGU Fall Meeting. Abstract 1455.
Kreslavsky, M.A., 2007. Statistical characterization of spatial distribution of impact craters: Implications to present-day cratering rate on Mars. LPI Contributions, 1353. Abstract 3325.
Kulik, L.A., 1927. On the fall of the Podkamennaya Tunguska meteorite in 1908. J. Russ. Acad. Sci. 23, 399–402.
Laskar, J., Correia, A.C.M., Gastineau, M., Joutel, F., Levrard, B., Robutel, P., 2004. Long term evolution and chaotic diffusion of the insolation quantities of Mars. Icarus 170, 343–364. http://dx.doi.org/10.1016/j.icarus.2004.04.005.
Malin, M.C., Edgett, K.S., Posiolova, L.V., McColley, S.M., Dobrea, E.Z.N., 2006. Present-day impact cratering rate and contemporary gully activity on Mars. Science 314, 1573–1577.
Malin, M.C. et al., 2007. Context Camera investigation on board the Mars Reconnaissance Orbiter. J. Geophys. Res. 112, 5. http://dx.doi.org/10.1029/2006JE002808.
McEwen, A.S., Bierhaus, E.B., 2006. The importance of secondary cratering to age constraints on planetary surfaces. Annu. Rev. Earth Planet. Sci. 34, 535–567.
McEwen, A.S., Preblich, B.S., Turtle, E.P., Artemieva, N.A., Golombek, M.P., Hurst, M., Kirk, R.L., Burr, D.M., Christensen, P.R., 2005. The rayed crater Zunil and interpretations of small impact craters on Mars. Icarus 176, 351–381.
McEwen, A.S et al., 2007a. Mars Reconnaissance Orbiter's High Resolution Imaging Science Experiment (HiRISE). J. Geophys. Res. 112, 5. http://dx.doi.org/10.1029/2005JE002605.
McEwen, A.S., Grant, J.A., Tornabene, L.L., Byrne, S., Herkenhoff, K.E., 2007b. HiRISE observations of small impact craters on Mars. Lunar Planet. Sci. 38. Abstract 2009.
McEwen, A.S., Tornabene, L.L., Hirise Team, 2007c. Modern Mars: HiRISE observations of small, recent impact craters. LPI Contributions, 1353, 3086.
McEwen, A.S., Banks, M.E., Baugh, N., Becker, K., Boyd, A., Bergstrom, J.W., Beyer, R.A., Bortolini, E., Bridges, N.T., Byrne, S., Castalia, B., Chuang, F.C., Crumpler, L.S., Daubar, I., Davatzes, A.K., Deardorff, D.G., Dejong, A., Delamere, W.A., Dobrea, E.N., Dundas, C.M., Eliason, E.M., Espinoza, Y., Fennema, A., Fishbaugh, K.E., Forrester, T., Geissler, P.E., Grant, J.A., Griffes, J.L., Grotzinger, J.P., Gulick, V.C., Hansen, C.J., Herkenhoff, K.E., Heyd, R., Jaeger, W.L., Jones, D., Kanefsky, B., Keszthelyi, L., King, R., Kirk, R.L., Kolb, K.J., Lasco, J., Lefort, A., Leis, R., Lewis, K.W., Martinez-Alonso, S., Mattson, S., McArthur, G., Mellon, M.T., Metz, J.M., Milazzo, M.P., Milliken, R.E., Motazedian, T., Okubo, C.H., Ortiz, A., Philippoff, A.J., Plassmann, J., Polit, A., Russell, P.S., Schaller, C., Searls, M.L., Spriggs, T., Squyres, S.W., Tarr, S., Thomas, N., Thomson, B.J., Tornabene, L.L., van Houten, C., Verba, Weitz, C.M., Wray, J.J., 2010. The High Resolution Imaging Science Experiment (HiRISE) during MRO's Primary Science Phase (PSP). Icarus 205, 2–37. http://dx.doi.org/10.1016/j.icarus.2009.04.023.
McKinnon, W.B., Zahnle, K.J., Ivanov, B.A., Melosh, H.J., 1997. Cratering on Venus: Models and observations. In: Bougher, S.W., Hunten, D.M., Phillips, R.J. (Eds.), Venus II. University of Arizona Press, Tucson, Arizona, pp. 969–1014.
Michael, G.G., Neukum, G., 2010. Planetary surface dating from crater size–frequency distribution measurements: Partial resurfacing events and statistical age uncertainty. Earth Planet. Sci. Lett. 294, 223–229. http://dx.doi.org/10.1016/j.epsl.2009.12.041.
Neukum, G., Ivanov, B.A., 1994. Crater size distributions and impact probabilities on Earth from lunar, terrestrial-planet, and asteroid cratering data. In: Gehrels, T., Matthews, M.S., Schumann, A. (Eds.), Hazards Due to Comets and Asteroids. University of Arizona Press, Tucson, AZ, pp. 359–416.
Neukum, G., Ivanov, B.A., Hartmann, W.K., 2001. Cratering records in the inner Solar System in relation to the lunar reference system. Space Sci. Rev. 96, 55–86.
Neukum, G. et al., 2010. The geologic evolution of Mars: Episodicity of resurfacing events and ages from cratering analysis of image data and correlation with radiometric ages of martian meteorites. Earth Planet. Sci. Lett. 294 (3–4), 204–222. http://dx.doi.org/10.1016/j.epsl.2009.09.006.
Öberst, J., Nakamura, Y., 1991. A search for clustering among the meteoroid impacts detected by the Apollo lunar seismic network. Icarus 91, 315–325.
Popova, O., Nemtchinov, I., Hartmann, W.K., 2003. Bolides in the present and past martian atmosphere and effects on cratering processes. Meteorit. Planet. Sci. 38, 905–925. http://dx.doi.org/10.1111/j.1945-5100.2003.tb00287.x.
Popova, O.P., Hartmann, W.K., Nemtchinov, I.V., Richardson, D.C., Berman, D.C., 2007. Crater clusters on Mars: Shedding light on martian ejecta launch conditions. Icarus 190, 50–73. http://dx.doi.org/10.1016/j.icarus.2007.02.022.
Popova, O. et al., 2011. Very low strengths of interplanetary meteoroids and small asteroids. Meteorit. Planet. Sci. 46, 1525–1550, http://dx.doi.org/10.1111/j.1945-5100.2011.01247.x.
Robbins, S.J., Hynek, B.M., 2011. Distant secondary craters from Lyot crater, Mars, and implications for surface ages of planetary bodies. Geophys. Res. Lett. 38, 5201. http://dx.doi.org/10.1029/2010GL046450.
Ruff, S.W., Christensen, P.R., 2002. Bright and dark regions on Mars: Particle size and mineralogical characteristics based on Thermal Emission Spectrometer data. J. Geophys. Res. 107, 1–22. http://dx.doi.org/10.1029/2001JE001580.
Shoemaker, E.M., 1965. Preliminary analysis of the fine structure of the lunar surface in Mare Cognitum, JPL Tech. Report No. 32-700. In: Hess, W.N., Menzel, D.H., O'Keefe, J.A. (Eds.), The Nature of the Lunar Surface. Johns Hopkins Press, Baltimore, pp. 23–77.
Silvestro, S., Fenton, L.K., Vaz, D.A., Bridges, N.T., Ori, G.G., 2010. Ripple migration and dune activity on Mars: Evidence for dynamic wind processes. Geophys. Res. Lett. 37, L20203. http://dx.doi.org/10.1029/2010GL044743.
Stöffler, D., Ryder, G., 2001. Stratigraphy and isotope ages of lunar geologic units: Chronological standard for the inner Solar System. Space Sci. Rev. 96, 9–54.
Strom, R.G. et al., 2011. Mercury crater statistics from MESSENGER flybys: Implications for stratigraphy and resurfacing history. Planet. Space Sci. 59, 1960–1967. http://dx.doi.org/10.1016/j.pss.2011.03.018.
Tera, F., Papanastassiou, D.A., Wasserburg, G.J., 1974. Isotopic evidence for a terminal lunar cataclysm. Earth Planet. Sci. Lett. 22, 1–21.
Thomas, P., Veverka, J., 1980. Crater densities on the satellites of Mars. Icarus 41, 365–380. http://dx.doi.org/10.1016/0019-1035(80)90221-3.
Werner, S.C., Ivanov, B.A., Neukum, G., 2009. Theoretical analysis of secondary cratering on Mars and an image-based study on the Cerberus Plains. Icarus 200, 406–417. http://dx.doi.org/10.1016/j.icarus.2008.10.011.
Werner, S.C., Tanaka, K.L., 2011. Redefinition of the crater-density and absolute-age boundaries for the chronostratigraphic system of Mars. Icarus 215, 603–607. http://dx.doi.org/10.1016/j.icarus.2011.07.024.
Wiens, G., La Paz, L., 1935. On the fall of the Podkamennaya Tunguska meteorite in 1908, by L. Kulik, translation. Popul. Astron. 43, 596–599.
Wilhelms, D.E., McCauley, J.F., Trask, N.J., 1987. The Geologic History of the Moon. USGS, Washington.
Williams, J.-P., Pathare, A., Aharonson, O., 2012. Modelling small impact crater populations on Mars. Euro. Planet. Sci. Congr., 7, 95, (abstract).
Xiao, Z., Strom, R.G., 2012. Problems determining relative and absolute ages using the small crater population. Icarus 220 (1), 254–267. http://dx.doi.org/10.1016/j.icarus.2012.05.012.
Zappala, V., Cellino, A., Gladman, B.J., Manley, S., Migliorini, F., 1998. Asteroid showers on Earth after family breakup events. Icarus 134, 176–179. http://dx.doi.org/10.1006/icar.1998.5946.